L-vacancy production in near-symmetric heavy-ion collisions ($Z \gtrsim 35$)

W. E. Meyerhof
Department of Physics, Stanford University, California 94305

A. Rüetschi,* Ch. Stoller, M. Stöckli, and W. Wölfli
Nuclear Physics Laboratory, Swiss Federal Institute of Technology, CH—8093 Zurich, Switzerland
(Received 1 February 1979)

The authors have measured the projectile and target L x-ray spectra and cross sections for 41-MeV Ta projectiles bombarding thin targets between Ag and Th and for 17–60-MeV collisions of Ho on Ho, Au on Au, Pb on Pb, and U on Th. These cross sections, as well as those measured elsewhere, are examined in terms of a simple vacancy-sharing model involving the $4f\sigma$ and $3d\sigma$ molecular orbitals (MO). From the $L\beta_1/L\alpha$ x-ray intensity ratios it is found that in symmetric collisions the $4f\sigma$ MO correlates to the $2p_{3/2}$ level of the collision partners (correlation rule of Barat and Lichten). As the asymmetry of the collision system increases, there is an increasing tendency for the $4f\sigma$ MO to correlate to the $2s$ level of the lower-Z collision partner (correlation rule of Eichler and collaborators). The physical basis for the shift of the $4f\sigma$ MO correlation is discussed.

I. INTRODUCTION

A search of the literature reveals that to date only a few systematic measurements have been made of the L x-ray line structure and production cross sections in near-symmetric collisions with $Z \gtrsim 35$.[1] Notable is the work of Datz *et al.*[2] and of Hagmann *et al.*,[3] who bombarded a range of targets between $_6$C and $_{92}$U with 6–60-MeV $_{53}$I projectiles. Datz *et al.*[2] found strong variations in the $L\beta_1/L\alpha$ x-ray intensity ratio as a function of target Z, which point to quasimolecular effects involving level matching. Hagmann *et al.*[3] have attempted a quantitative explanation of the variation in terms of avoided molecular-orbital (MO) level crossings.

In order to extend the available data and to investigate the role of quasimolecular effects in near-symmetric high-Z collisions more fully, we made various measurements of projectile and target L x-ray spectra and cross sections. Using 41-MeV $_{73}$Ta projectiles, a variety of targets between $_{47}$Ag and $_{90}$Th were bombarded. Also some collision systems were studied as a function of projectile energy between 17 and 60 MeV: $_{67}$Ho→Ho, $_{79}$Au→Au, $_{82}$Pb→Pb, $_{92}$U→Th.[4]

The thrust of our work in the framework of the present understanding of L-shell vacancy production is as follows. If a series of targets (Z_t) is bombarded with a given projectile (Z_p) at a fixed bombarding energy (E_p), regular variations of the cross-section magnitude with Z_t are found in the target and projectile cross sections, whenever the inner-shell binding energies of the two collision partners happen to match.[5–7] Such level-matching effects in L x-ray production have been investigated by Kavanagh *et al.*[8] Using the work of Barat and Lichten[9] on electron promotion, Fortner[10] has shown also that in near-symmetric collisions, vacancies are brought into the L levels of the collision partners via the $4f\sigma$ MO. This orbital correlates to the L levels of the lower-Z collision partner (see Fig. 1, adapted from Ref.

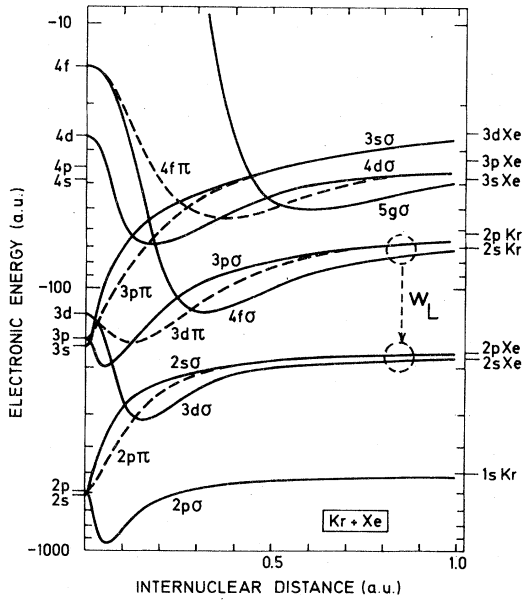

FIG. 1. Diabatic correlation diagram for an asymmetric collision ($_{36}$Kr+$_{54}$Xe) according to Eichler *et al.* (Ref. 11). The vertical dashed line indicates the vacancy-sharing process examined in this paper. The vacancy-sharing probability w_L is discussed in Sec. III A.

11). From the L-vacancy production in the higher-Z partner, Fortner[10] could show that $3d\sigma$-vacancy production is at least an order of magnitude smaller than the $4f\sigma$-vacancy production in the systems investigated by him ($E_p = 15-200$ keV, $Z_p = 15-19$, $Z_t = 6, 18$). Since these systems are relatively light, fluorescence effects inhibited accurate determinations of vacancy cross sections.

As the L levels of the higher-Z and lower-Z partners approach, one expects vacancy sharing to take place on the outgoing part of the collision due to the long-range radial coupling between the MO's correlating to the L levels of the two partners, similar to that found for the K levels.[12-14] (L-vacancy sharing on the ingoing part of a collision has already been established by the work of Lennard and Mitchell.[15]) Since six L levels come into play in the vacancy-sharing process, the situation is even more complex than in K-L vacancy sharing which involves four levels.[16] For this reason we have applied a simple model to the L-L vacancy sharing process, which despite its schematic nature leads to a reasonable understanding of L-vacancy production in near-symmetric collisions. The model assumes that the relevant inner-shell vacancies are formed in the $4f\sigma$ MO by ionization[17] or electron promotion[9,10] at small internuclear distances in single- or multiple-collision processes and that on the outgoing part of the collision long-range radial coupling of the Demkov form[12,18] distributes the vacancies between the various MO's leading to the separated atom (SA) L levels. (In the K-L level matching case[16] a more flexible model[19] had to be used, but such a model would introduce too many arbitrary parameters here. See also Ref. 20.)

Our model indicates that in symmetric collisions the $4f\sigma$ MO correlates to the $2p_{3/2}$ SA level, as originally proposed by Barat and Lichten,[9] and not to the $2s$ SA level as suggested by Eichler *et al.*[11] for high-Z systems. On the other hand, if the collision system is asymmetric, the correlation of the $4f\sigma$ MO seems to shift toward the $2s$ SA level of the lower-Z collision partner, in accord with the suggestion of Eichler *et al.*[11]

We do not have a model to represent the primary $4f\sigma$-vacancy production, but show that the cross-section scales in a manner similar to that found for $2p\sigma$- and $3d\sigma$-vacancy production.[17,21] Hence, similar mechanisms might operate in all these cases. As in $3d\sigma$-vacancy production, there is no clear evidence for multiple-collision effects.[16,17]

In Sec. II, experimental details are given. Experimental results are related to our vacancy-sharing model in Sec. III. A scaling law for the $4f\sigma$ cross section is given in Sec. IV. A physical basis for the findings of Sec. III is discussed in Sec. V.

II. EXPERIMENT

The 6-MV tandem Van de Graaff accelerator of the Swiss Federal Institute of Technology was used to produce beams of 17–60-MeV $_{67}$Ho, $_{73}$Ta, $_{79}$Au, $_{82}$Pb, and $_{92}$U. Targets of 20–50 μg/cm^2 thick $_{50}$Sn, $_{62}$Sm, Ho, Ta, Au, Pb and $_{90}$ThF, deposited on 20-μg/cm^2 C foils and self-supporting targets of 90-μg/cm^2 $_{47}$Ag and 150-μg/cm^2 Au were mounted in a 25-cm-diam target chamber at 45° to the beam direction. The x rays passed through 50–300-μm Al absorbers and a 37-μm Be window before entering a 80-mm^2 × 5-mm Si(Li) detector placed at 90° to the beam. The particle current was determined by Rutherford scattering of the beam by the target foils into a surface-barrier detector at 30° to the beam. Counts due to recoiling C atoms from the target backing were eliminated by pulse-height analysis.

X-ray cross sections could be obtained directly from the x-ray and particle counts, by comparison with the screened Rutherford cross section integrated over the face of the detector. Corrections were made for deadtime, absorption, detection efficiency and for a continuum background under the characteristic x-ray lines. For the Ho and Au beams, separate measurements were made of the projectile x-ray production by the C backing foil: this was always less than 2% of the x-ray yield due to the heavy-atom targets. Typical errors for the total L x-ray cross sections were between 2% and 10%. A computer program was used to separate the L x-ray spectra into $Ll, L\alpha, L\beta(1)$, $L\beta(2)$ and $L\gamma$ line groups.[2,3,16] The relevant groups are defined in Sec. III B. Because of possible systematic errors introduced in the separation procedure, we assign a maximum uncertainty of ±30% to the absolute line-group cross sections. Further experimental details are described in Ref. 4.

For comparison with a theoretical model it is necessary to relate the experimental line-group cross sections to the cross sections for primary vacancy production in L_1, L_2, and L_3 subshells of each collision partner. Details of this procedure are discussed in Sec. III B below and in Appendix A of Ref. 16. Here we mention only that uncertainties in the fluorescence yields and in the Coster-Kronig transition probabilities caused by solid-target effects may cause overestimates in vacancy-production cross sections by as much as a factor of 2 (see Ref. 16 and Sec.

II of Ref. 17). Since we use mainly cross-section ratios in comparisons with our model, the error should be considerably smaller. In view of the fact that our model is schematic, it did not seem worthwhile to use more refined methods of cross-section analysis, such as those employed by Hagmann *et al.*[3]

Figure 2 gives an overview of our total L-vacancy cross sections for the 41-MeV $_{73}$Ta beam[4] as a function of target Z and compares these with 43-MeV $_{35}$Br and 47-MeV $_{53}$I cross sections.[16] In the L-L level matching region, i.e., near symmetry, the cross section trends in all three cases are similar. A quantitative discussion is given in Sec. III A. Results for L-subshell cross-section ratios are presented and examined in Secs. III B and III C.

III. L-L VACANCY-SHARING MODEL

A. Total L cross sections

As mentioned in Sec. II, we assume that vacancies created in the $4f\sigma$ MO at small internuclear distances are shared on the outgoing part of the collision between the MO's leading to the SA L levels. If one does not differentiate the SA L subshells, one can define an overall vacancy-sharing probability w_L indicated in Fig. 1. The total L-vacancy cross sections of the two collision partners can then be evaluated in terms of the MO-vacancy cross sections, analogous to the K-K vacancy sharing case [Eqs. (2) and (3) of Ref. 22]:

$$\sigma_L(h) = (1 - w_L)\sigma(3d\sigma) + w_L\sigma(4f\sigma)\,, \tag{1}$$

$$\sigma_L(l) = w_L\sigma(3d\sigma) + (1 - w_L)\sigma(4f\sigma) + \sigma_{L-M}\,, \tag{2}$$

where $\sigma_L(h)$ and $\sigma_L(l)$ are the L-vacancy-production cross sections of the higher-Z and lower-Z collision partners, respectively. In Eqs. (1) and (2) we have included the possibility that vacancies created in the $3d\sigma$ MO can also end up in the SA L levels[9,10] (see Fig. 1). In analogy with the K-K vacancy-sharing case[22] we have assumed that the vacancy-sharing probabilities for the $4f\sigma$ and $3d\sigma$ MO's are identical. We have also envisaged the possibility that for sufficiently asymmetric collision the lower-Z collision partner can obtain vacancies from the $5g\sigma$ MO (see Fig. 1), producing an additional cross section σ_{L-M}. This cross section is expected to dominate $\sigma_L(l)$, if the $L(l)$ and $M(h)$ levels overlap,[8,9] leading to a situation analogous to K-L level matching.[16,20]

For near-symmetric collisions one finds experimentally[10,16]

$$\sigma(3d\sigma) \ll \sigma(4f\sigma)\,, \quad \sigma_{L-M} \ll \sigma(4f\sigma)\,, \tag{3}$$

so that Eqs. (1) and (2) then yield

$$\sigma_L(h) + \sigma_L(l) \cong \sigma(4f\sigma)\,, \tag{4}$$

$$\sigma_L(h)/\sigma_L(l) \cong w_L/(1 - w_L)\,. \tag{5}$$

These equations allow one to test experimentally model calculations of $\sigma(4f\sigma)$ and of w_L. The $4f\sigma$ cross section is discussed in Sec. IV. Here we concentrate on w_L.

It is tempting to apply the model calculation of the K-K vacancy-sharing probability[12] to L-L vacancy sharing, since in both cases one deals with near-symmetric collisions. Such a step would be particularly justified, if L-vacancy sharing takes place mainly between identical subshells of the collision partners: $L_1(l) \leftrightarrow L_1(h)$, etc. (It turns out that this is *not* the case.) Then

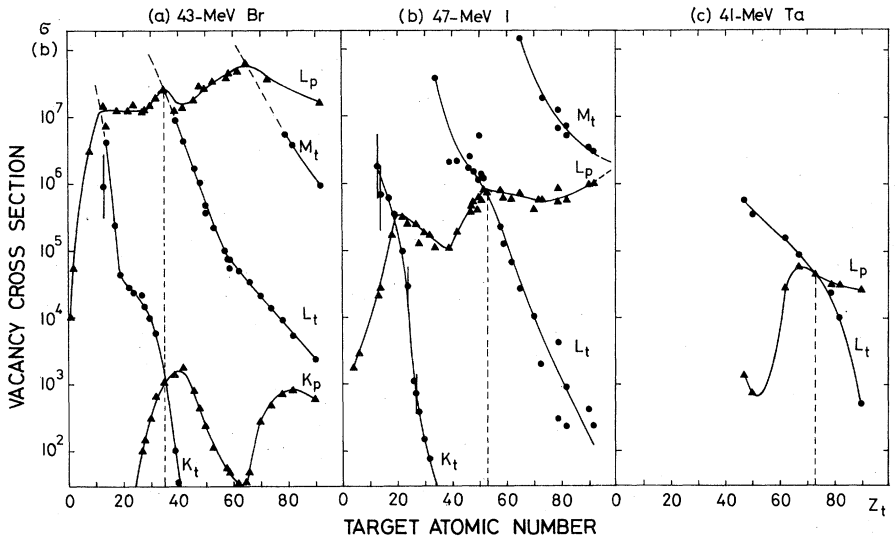

FIG. 2. Vacancy cross sections plotted as a function of target atomic number for (a) 43-MeV $_{35}$Br (Ref. 16), (b) 47-MeV $_{53}$I (Ref. 16), and (c) 41-MeV $_{73}$Ta (Ref. 4). Capital letters refer to the shells (subshells are not distinguished) and the subscripts to projectile (p) and target (t). Dashed vertical lines indicate symmetric collisions.

one finds from Ref. 12,

$$w_L/(1-w_L)=\exp(-2x_L)\,, \tag{6}$$

where

$$2x_L=\pi(I_h^{1/2}-I_l^{1/2})/(\tfrac{1}{2}mv_p^2)^{1/2}\,. \tag{7}$$

Here I_h and I_l are the L-ionization energies of the higher-Z and lower-Z collision partners, m is the electron mass and v_p the projectile velocity.

In Fig. 3, we compare Eq. (6) with our[4] and other[16,23] data for $_{47}$Ag, $_{53}$I, $_{73}$Ta, and $_{92}$U projectiles bombarding various targets near symmetry. We have made two different assumptions for I_h and I_l. In Fig. 3(a), I_h and I_l were chosen to be the L_2-subshell binding energies of each partner (L_1 or L_3 could have been used equally well), corresponding to the assumption that vacancy sharing takes place mainly between identical subshells. In Fig. 3(b), I_h and I_l were chosen to be equal to the L_3 binding energy of the higher-Z partner and the L_1 binding energy of the lower-Z partner, respectively, corresponding to the assumption that vacancy sharing depends primarily on the energy separation of the MO's leading to the SA levels and less on their electronic configurations. One sees from Fig. 3(b), that the latter choice for I_h and I_l gives a much better agreement with Eq. (6), than the former. This leads to two conclusions. First, energy separation between MO's appears to be the most important quantity determining vacancy sharing. Second, in near-symmetric collisions the Demkov model[12,18] may be used to estimate vacancy-sharing ratios. This model takes into account, albeit schematically, the energy separation between levels which couple.

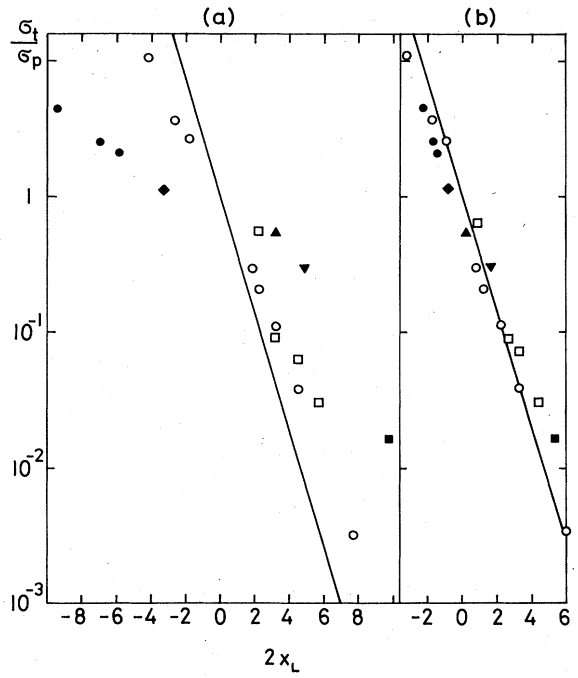

FIG. 3. Target-to-projectile L-vacancy cross-section ratio for near-symmetric collisions vs scaling parameter $2x_L$ defined in Eq. (7). See text (Sec. III A) for difference between (a) and (b). Line is model prediction of Eq. (6). Symbols have the following meaning: ●23-58-MeV $_{92}$U+$_{82}$Pb (Ref. 4); ♦,▲, ▼, ■, 41-MeV $_{73}$Ta+$_{67}$Ho, $_{79}$Au, $_{82}$Pb, $_{90}$Th (Ref. 4), O 47-MeV $_{53}$I projectiles on various targets (Ref. 16), □ 15-MeV $_{47}$Ag projectiles on various targets (Ref. 23).

B. L-subshell cross sections

1. *Symmetric collisions*

We were able to obtain experimentally cross sections for Ll, $L\alpha$, $L\beta(1)$, $L\beta(2)$, and $L\gamma$ line groups for various symmetric collision systems. As discussed in Appendix A of Ref. 16, the Ll, $L\alpha$, and $L\beta(2)$ cross sections all reflect transition probabilities to the L_3 subshell, so that only one of these cross sections, e.g., $L\alpha$ is sufficient to examine L_3-vacancy production. The $L\beta(1)$ and $L\gamma$ x-ray cross sections reflect combinations of transitions to the L_1 and L_2 subshells, unfortunately with similar relative transition probabilities. Therefore, one cannot extract the individual L_1- and L_2-vacancy production cross section from these groups.[24] But it is sufficient to examine one of these line groups, e.g., $L\beta(1)$, in order to obtain information on the combination of L_1- and L_2-vacancy production cross sections.

Calling σ_1, σ_2, and σ_3 the primary L_1-, L_2-, and L_3-subshell vacancy-production cross sections, and σ_2' and σ_3' the Coster-Kronig altered cross sections, one finds for the $L\alpha$ and $L\beta(1)$ line group x-ray cross sections.[3,16,25]

$$\sigma_\alpha=\sigma_3'\omega_3(\Gamma_{3,M4}+\Gamma_{3,M5})/\Gamma_3\,, \tag{8}$$

$$\sigma_{\beta(1)}=\frac{\sigma_2'\omega_2\Gamma_{2,M4}}{\Gamma_2}+\frac{\sigma_1\omega_1(\Gamma_{1,M2}+\Gamma_{1,M3})}{\Gamma_1}\,, \tag{9}$$

$$\equiv\sigma_2''\omega_2\Gamma_{2,M4}/\Gamma_2\,. \tag{10}$$

Here

$$\sigma_3'=\sigma_3+f_{23}\sigma_2+(f_{12}f_{23}+f_{13})\sigma_1\,, \tag{11}$$

$$\sigma_2''=\sigma_2'+r\sigma_1=\sigma_2+(f_{12}+r)\sigma_1\,, \tag{12}$$

$$r=\frac{\omega_1(\Gamma_{1,M2}+\Gamma_{1,M3})/\Gamma_1}{\omega_2\Gamma_{2,M4}/\Gamma_2}\,. \tag{13}$$

In Eqs. (8)–(13), ω_i and Γ_i are the fluorescence yield[25] and total radiative width[26] of the subshell L_i, Γ_{ik} is the partial radiative width[26] for the transition from a higher subshell k to the subshell L_i, and f_{ij} is the Coster-Kronig transition prob-

ability[25] from subshell L_i to subshell L_j. The $\beta(1)/\alpha$ x-ray intensity ration, which turns out to be useful for our purposes, is given by

$$\beta(1)/\alpha \equiv \sigma_{\beta(1)}/\sigma_\alpha \tag{14}$$

$$= \Omega \frac{\sigma_2 + (f_{12}+r)\sigma_1}{\sigma_3 + f_{23}\sigma_2 + (f_{12}f_{23}+f_{13})\sigma_1}, \tag{15}$$

where

$$\Omega = \frac{\omega_2 \Gamma_{2,M4}/\Gamma_2}{\omega_3(\Gamma_{3,M4}+\Gamma_{3,M5})/\Gamma_3}. \tag{16}$$

The consequences of substituting tabulated single-vacancy fluorescence yields,[25] Coster-Kronig transition probabilities[25] and radiative widths[26] in Eqs. (8)–(16) has been discussed extensively in Appendix A of Ref. 16 and in Ref. 17 and comparisons with experiment are presented in Refs. 16 and 24. One may expect up to a "factor of three" systematic errors in computed cross sections, but considerably smaller errors in computed cross ratios, such as Eq. (14). We consider such systematic errors acceptable, since we shall be interested often in trends with atomic number or bombarding energy rather than in absolute values. Hence, in view of the great convenience of using the tabulations,[25,26] single-vacancy values for ω, f and Γ are used throughout this paper. With these values one finds that in the Z region of interest here ($47 \leq Z < 92$), $r \cong 0.45$ [Eq. (13)] and $\Omega \cong 1.0$ [Eq. (16)].

For comparison with the model calculations, discussed below, we introduce the experimentally determined vacancy fractions

$$v_3 = \sigma_3'/\sigma_L, \tag{17}$$

$$v_2 = \sigma_2''/\sigma_L. \tag{18}$$

Here σ_3' is obtained from σ_α, σ_2'' is obtained from $\sigma_{\beta(1)}$ and σ_L is the total L-vacancy production cross section

$$\sigma_L = \sigma_1 + \sigma_2 + \sigma_3 \tag{19}$$

$$= (\sigma_l + \sigma_\alpha + \sigma_{\beta(1)} + \sigma_{\beta(2)} + \sigma_\gamma)/\bar{\omega}_L. \tag{20}$$

One finds[16] that $\omega_L \cong \omega_3$.

Using a model similar to that applied in Ref. 16, we now assume that in a symmetric collision, vacancies produced in the $4f\sigma$ MO at small internuclear distances are shared between the L *subshells* of the collision partners in ratios predicted by the two-state Demkov vacancy-sharing model of Ref. 12. The application of a two-state model to a many-level situation is justifiable only, if the ignored couplings, e.g., in the Barat-Lichten scheme [Fig. 4(a)] between the MO's correlating to the L_1 and L_2 levels, are indeed small. This is difficult to know *a priori*. It may also be questioned whether the Demkov model is applicable at all to couplings between MO's which lead to subshells of the same collision partner, although a similar model was applied successfully in this manner in Ref. 16. One reason for the success may be that, as Nikitin has shown,[19] many different forms of radial coupling lead to a vacancy-sharing ratio close in form to that of Demkov's model. In each case a characteristic energy gap between the MO's enters into an exponential factor. As a result, the MO energy separation turns out to be the most critical quantity for the vacancy-sharing ratio, in accord with the findings of Sec. III A.

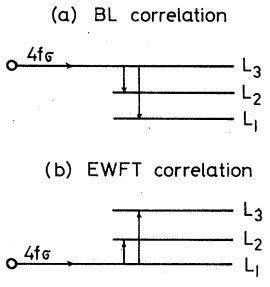

FIG. 4. Schematic $4f\sigma$-correlation proposals considered in the model calculations for symmetric collisions. Vertical arrows indicate vacancy-sharing transitions considered in the model. Subsequent Coster-Kronig transitions are not shown, but are taken into account. (a) Proposal of Barat and Lichten (Ref. 9). (b) Proposal of Eichler *et al.* (Ref. 11).

We distinguish two possible correlations of the $4f\sigma$ MO to the L subshells, as sketched in Fig. 4: the Barat-Lichten (BL) proposal,[9] that the $4f\sigma$ MO correlates to the L_3 subshell [Fig. 4(a)], and the Eichler-Wille-Fastrup-Taulbjerg (EWFT) proposal,[11] that the $4f\sigma$ MO correlates to the L_1 subshell [Fig. 4(b)]. For the BL correlation, the model then gives

$$\sigma_1/\sigma_L = [\exp(-2x_{31})]/\Sigma_B, \tag{21}$$

$$\sigma_2/\sigma_L = [\exp(-2x_{32})]/\Sigma_B, \tag{22}$$

$$\sigma_3/\sigma_L = 1/\Sigma_B, \tag{23}$$

where

$$\Sigma_B = 1 + \exp(-2x_{31}) + \exp(-2x_{32}). \tag{24}$$

Similarly, for the EWFT proposal,

$$\sigma_1/\sigma_L = 1/\Sigma_E, \tag{25}$$

$$\sigma_2/\sigma_L = [\exp(-2x_{21})]/\Sigma_E, \tag{26}$$

$$\sigma_3/\sigma_L = [\exp(-2x_{31})]/\Sigma_E, \tag{27}$$

where

$$\Sigma_E = 1 + \exp(-2x_{21}) + \exp(-2x_{31}). \tag{28}$$

In these equations,

$$2x_{ij} = \pi/|I_i^{1/2} - I_j^{1/2}|/(\tfrac{1}{2}mv_p^2)^{1/2}, \tag{29}$$

where I_i and I_j are the L_i and L_j subshell ionization energies, respectively.

To compare the model with experiment, Eqs. (21)–(24) or (25)–(28) must be substituted into Eqs. (15) or (17) and (18). One then finds for the BL proposal

$$\frac{\beta(1)}{\alpha} = \Omega \frac{\exp(-2x_{32}) + (f_{12}+r)\exp(-2x_{31})}{1+f_{23}\exp(-2x_{32}) + (f_{12}f_{23}+f_{13})\exp(-2x_{31})}, \tag{30}$$

and for the EWFT proposal

$$\frac{\beta(1)}{\alpha} = \Omega \frac{\exp(-2x_{21}) + f_{12} + r}{\exp(-2x_{31}) + f_{23}\exp(-2x_{21}) + f_{12}f_{23} + f_{13}}. \tag{31}$$

In Fig. 5 expressions (30) and (31) are compared with experimental values of $\beta(1)/\alpha$ from our[4] and other[2] work, as a function of Z, for a projectile energy of 41 MeV. In Fig. 6 a comparison is made as a function of projectile energy, for $Z = 47$, 67 and 82 (Refs. 4, 23 and 27). Despite the uncertainties caused by the use of single-vacancy values of ω, f and Γ in Eqs. (30) and (31), it is clear from Figs. 5 and 6 that our model is consistent only with the BL correlation scheme. To check whether the good agreement between the model calculation for the BL and experiment is fortuitous, we have varied the values of f and ω in accordance with the suggestions of Hagmann *et al.*[3] Although the EW-model values are quite sensitive to f and ω, the BL model values are very insensitive. This can also be seen in Fig. 5. Hence we can conclude that in symmetric collisions with $Z \gtrsim 47$ the $4f\sigma$ MO correlates to the L_3 subshell [Fig. 4(a)].

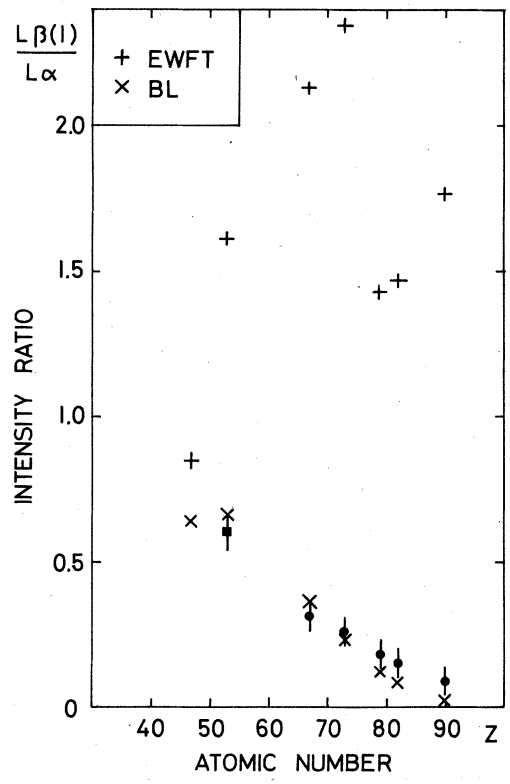

FIG. 5. $\beta(1)/\alpha$ x-ray intensity ratio for symmetric collisions as a function of the atomic number of the collision partners, for 41-MeV projectiles. Experimental points: ■ interpolated from Ref. 2, ● from Ref. 4. The large fluctuations in the EWFT model points are due to the use of single-vacancy Coster-Kronig transition probabilities.

2. *Asymmetric collisions*

In asymmetric collisions, one can obtain the cross sections σ_α and $\sigma_{\beta(1)}$ for each collision

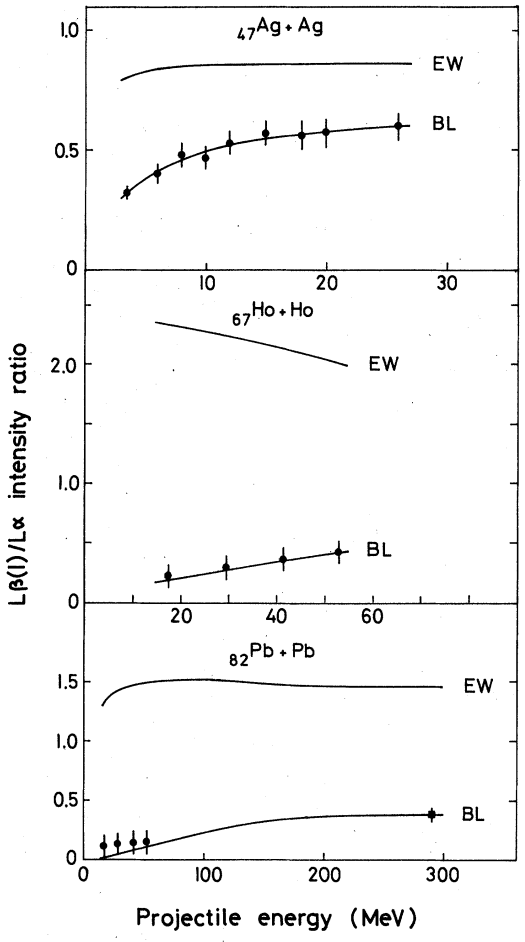

FIG. 6. $\beta(1)/\alpha$ x-ray intensity ratios for symmetric collisions as a function of the projectile energy. Experimental points: $_{47}$Ag+Ag from Ref. 23, $_{67}$Ho+Ho from Ref. 4, $_{82}$Pb+Pb ● from Ref. 4, ■ from Ref. 27. Curves marked BL and EW are the model results for the $4f\sigma$-correlation proposals of Ref. 9 and 11, respectively.

partner, but with considerable uncertainty, if the L spectra of the collision partners overlap. In Fig. 7 we show the target-Z (Z_t) dependence of the $\beta(1)/\alpha$ ratios for the projectile (p) and the target (t) for four different projectiles, each at a fixed bombarding energy.[2-4,23,27] Only the near-symmetric range of Z_t is presented. For convenience the symmetric values of Z_t have been lined up vertically. This makes it easy to recognize the qualitatively common trends in the Z_t dependence of the projectile and target ratios. We have also obtained experimental vacancy fractions from Eqs. (17) and (18). These are discussed below.

The model calculations for vacancy sharing in the asymmetric case are considerably more complicated than in the symmetric case. As Fig. 8 shows, one has to consider six subshells and, in our model, five vacancy-sharing ratios analogous to Eq. (6). Also, for sufficiently asymmetric collisions, vacancy feeding into the higher-Z L subshells from the $3d\sigma$ MO has to be taken into account. Eventually, vacancy feeding into the lower-Z L subshells due to L-M level matching would have to be included [see Eqs. (1) and (2)], but in the present work we avoid consideration of collisions which are so asymmetric that L-M level matching effects become appreciable.

Figure 8(a) sketches our model for the correlations and couplings according to the BL scheme,[9] and Fig. 8(b), according to the EWFT scheme.[11] In principle it is also possible for the $4f\sigma$ MO to correlate according to the BL scheme, and the $3d\sigma$ MO to correlate according to the EWFT scheme, and vice versa. With the help of Fig. 8, it is not difficult to write down the cross-section ratios for Z_l and Z_h analogous to Eqs. (21)–(23) and (25)–(27). As illustration we write down the cross-section ratio, $\sigma_2(h)/\sigma_L(\text{sum})$ in the BL scheme, where $\sigma_L(\text{sum})$ is the summed L-vacancy production cross section of both collision partners:

$$\sigma_L(\text{sum}) = \sigma(4f\sigma) + \sigma(3d\sigma)\,. \tag{32}$$

Let

$$\epsilon \equiv \sigma(3d\sigma)/\sigma(4f\sigma)\,. \tag{33}$$

Then

$$\frac{\sigma_2(h)}{\sigma_L(\text{sum})} = \frac{1}{1+\epsilon}\left(\frac{\exp(-2x_{3(l)2(h)})}{\Sigma_B(4f\sigma)} + \epsilon\,\frac{\exp(-2x_{3(h)2(h)})}{\Sigma_B(3d\sigma)}\right), \tag{34}$$

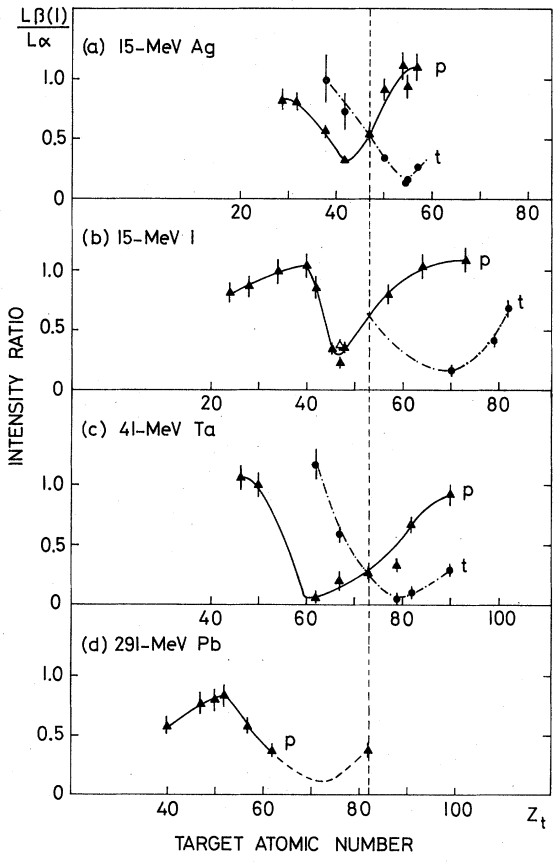

FIG. 7. $\beta(1)/\alpha$ x-ray intensity ratios for projectile (p) and target (t) atoms for various projectiles, as a function of the target atomic number. The abscissa in each case has been shifted so that the symmetric collisions are lined up with the dashed vertical line. Curves have been drawn to guide the eye. (a) 15-MeV $_{47}$Ag (Ref. 23), (b) ▲ 15-MeV $_{53}$I data from Ref. 2, Δ and ● 17-MeV I data from Ref. 3, (c) 41-MeV $_{73}$Ta (Ref. 4), (d) 291-MeV $_{82}$Pb (Ref. 27).

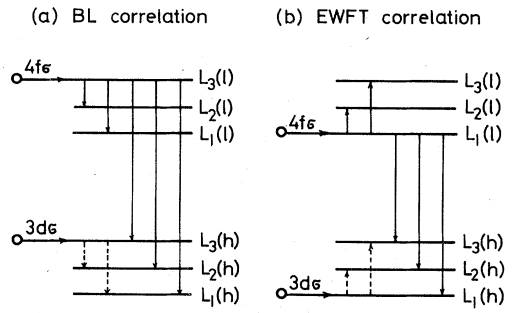

FIG. 8. Schematic correlation proposals used in the model calculations for asymmetric collisions. Vertical arrows indicate vacancy-sharing transitions considered in the model. Coster-Kronig transitions are not shown, but are taken into account. Symbols l and h refer to the lower-and higher-Z partners, respectively. (a) Proposal of Barat and Lichten (Ref. 9). (b) Proposal of Eichler *et al.* (Ref. 11).

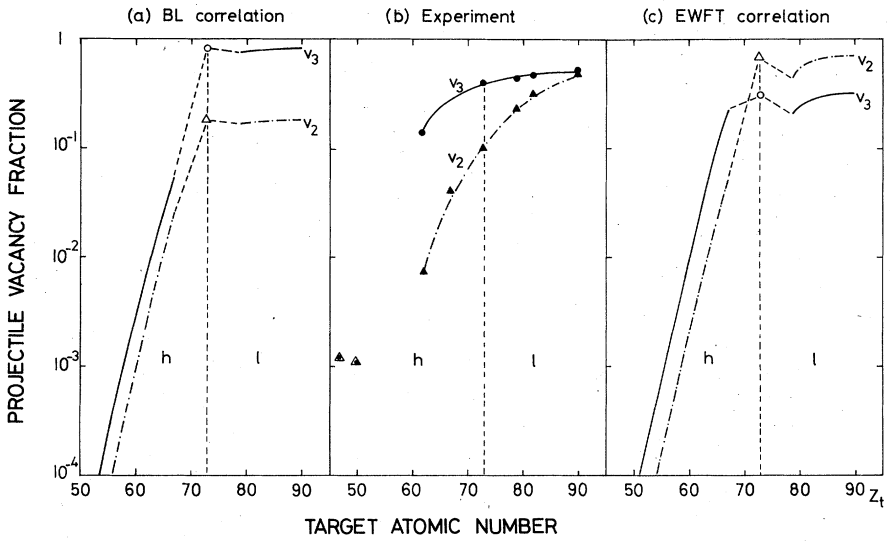

FIG. 9. Projectile L-shell vacancy fractions, defined by Eqs. (17) and (18), for 41-MeV $_{73}$Ta projectiles, plotted as a function of target atomic number. Vertical dashed lines indicate symmetric collisions. The symbols h and l denote the regions where the projectile is the higher- and lower-Z partner, respectively. (a) Model calculation using the proposal of Barat and Lichten [Fig. 8(a)], (b) experimental points (Ref. 4; typical errors ± 30%), (c) model calculation using proposal of Eichler *et al.* [Fig. 8 (b)].

where

$$\Sigma_B(3d\sigma) = 1 + \exp(-2x_{3(h)\,2(h)}) + \exp(-2x_{3(h)\,1(h)}) , \quad (35)$$

$$\Sigma_B(4f\sigma) = 1 + \exp(-2x_{3(l)\,2(l)}) + \cdots + \exp(-2x_{3(l)\,1(h)}) . \quad (36)$$

Each quantity $2x_{ij}$ is of the form of Eq. (29). Substitution of the ratios similar to Eq. (34) into equations analogous to Eqs. (15), (17) and (18) allows model estimates of $\beta(1)/\alpha$ ratios and of the vacancy fractions for each collision partner. From Fig. 2 one can estimate, by comparison with Fig. 10 of Ref. 16, that $\epsilon \cong 0.03$, 0.01 and 0.001 for 43-MeV Br, 47-MeV I, and 41-MeV Ta projectile-induced collisions, respectively.

In Fig. 9(b) we present the experimentally extracted projectile-vacancy fractions v_2 and v_3, Eqs. (17) and (18), with σ_L replaced by σ_L(sum), for 41-MeV Ta projectiles bombarding various targets.[4] In Figs. 9(a) and 9(c) we give the BL- and EWFT-model results, assuming $\epsilon = 0$. Figure 10 gives the experimental and model results for the target-vacancy fractions. In Figs. 9 and 10, triangles represent v_2 and circles v_3. The symbols h and l indicate the Z_t regions, separated by the vertical dashed symmetry line, where the particular atom, projectile or target, is the higher- or lower-Z partner. We have not applied the

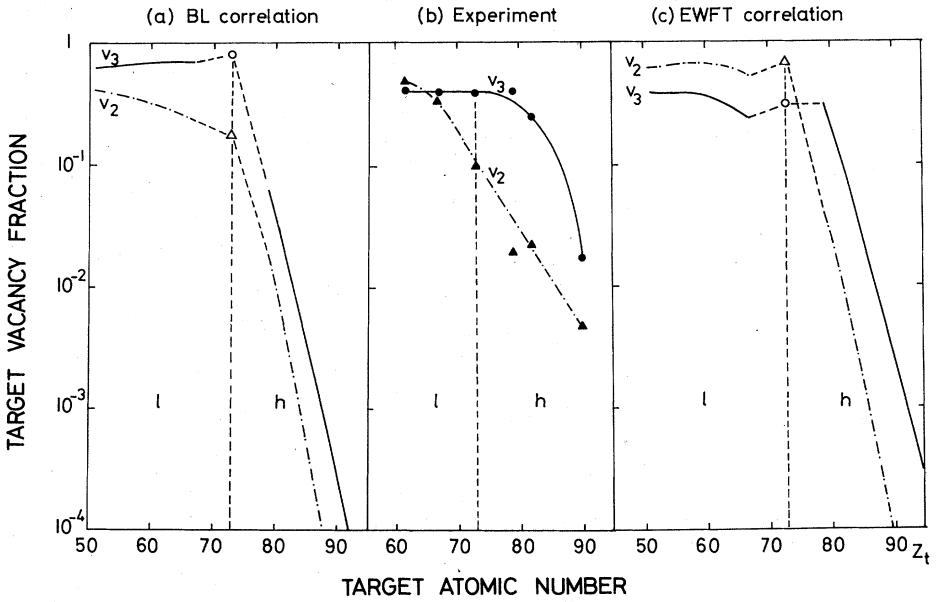

FIG. 10. Target L-shell vacancy fractions, defined by Eqs. (17) and (18) for 41-MeV $_{73}$Ta projectiles. The symbols h and l denote the region where the target is the higher-lower-Z partner respectively. Otherwise, caption is identical to that of Fig. 9.

model in the region where the L levels of the two partners overlap. The symmetric points for v_2 and v_3 are simply connected by dashed lines with the sufficiently asymmetric points.

Before discussing Figs. 9 and 10, we note from Eqs. (8)–(12) and (15)–(18) that, for each partner,

$$\beta(1)/\alpha = \Omega v_2/v_3 . \tag{37}$$

Hence, the experimental points in Figs. 9(b) and 10(b) are directly related to the data shown in Fig. 7(c).

From Figs. 9 and 10 one can see that the model predictions are qualitatively different for the BL and the EWFT proposals. In the BL scheme, v_2/v_3 is always less than unity, or $\beta(1)/\alpha < 1$ (since $\Omega \cong 1.0$), both for Z_h and Z_l. In the EWFT scheme, v_2/v_3 is less than unity for Z_h, but greater than unity for Z_l. The experimental fractions cannot distinguish between two schemes on the Z_h side, but on the Z_l side there is a clear trend from $v_2/v_3 < 1$ to $v_2/v_3 \gtrsim 1$, as the asymmetry of the collision increases. Figure 7 shows that this trend occurs not only for 41-MeV Ta, but is quite general (in this figure the projectile is the lower-Z partner for $Z_t > Z_p$ and the target for $Z_t < Z_p$).

Keeping in mind the limitations of our model, it appears then that with increasing asymmetry of the collision, the diabatic correlation of the $4f\sigma$ MO moves from the L_3 level in the symmetric situation (Sec. III A) toward the lower-Z L_1 level, i.e., toward the EWFT proposal (Fig. 1). In Sec. V we attempt to explain this shift in the correlation in terms of physical features of avoided crossings of the adiabatic MO's correlating to the lower-Z L_3 and L_1 levels. This is similar to the treatment of Hagmann *et al.*,[3] but they did not take into account any long-range radial coupling between the MO's represented here by "vacancy sharing."

If avoided crossings enter the picture, one would expect the crossing probability to be velocity dependent and to increase with increasing projectile velocity. Figure 11 shows the projectile energy dependence of the lower-Z $\beta(1)/\alpha$ ratio for $_{47}$Ag+ $_{57}$La (Ref. 23) and for $_{53}$I+ $_{64}$Gd, $_{70}$Y (Refs. 2 and 3). It appears that at least at higher projectile velocities, the correlation approaches the EWFT scheme.

We return to Figs. 9 and 10 and consider the higher-Z partner. The model calculations with $\epsilon = 0$ [Eq. (33)] predict that v_2 and v_3 should decrease rapidly with increasing asymmetry of the collision. Experimentally one finds that for 41-MeV Ta, v_2 and v_3 do not decrease below $\sim 10^{-3}$

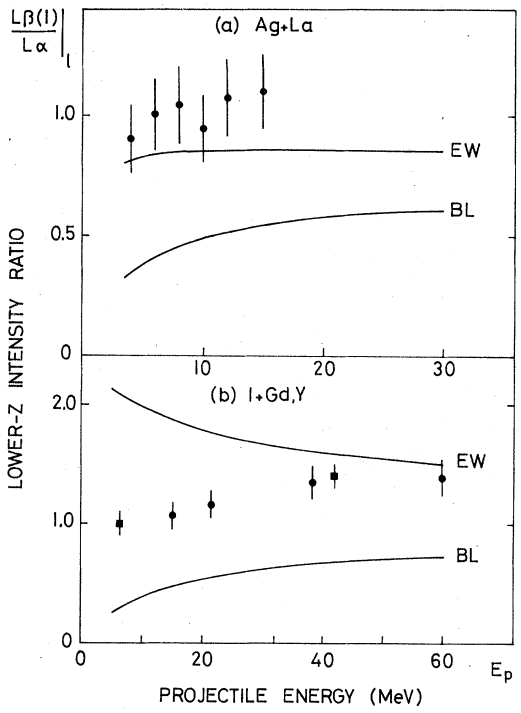

FIG. 11. $\beta(1)/\alpha$ x-ray intensity ratio for the lower-Z partner as a function of the atomic number. (a) $_{47}$Ag + $_{57}$La (Ref. 23), (b) $_{53}$I + $_{64}$Gd, $_{70}$Y (● from Ref. 2, ■ from Ref. 3). The curves marked BL and EW are the model results for the correlation proposals of Refs. 9 and 11, respectively.

[Fig. 9(b)]. Furthermore, the model predicts that $(v_2/v_3)_h \cong [\beta(1)/\alpha]_h \leq 0.3$, whereas experimentally $[\beta(1)/\alpha]_h$ reaches values close to unity, as the asymmetry increases (Fig. 7). These facts can be explained only, if one assumes $\epsilon \neq 0$, i.e., vacancy feeding from the $3d\sigma$ MO into the higher-Z L levels[10] (Figs. 1 and 8). One can then apply the model calculations in order to check whether the $3d\sigma$ MO correlates according to the BL proposal[9] [Fig. 8(a)] or according to the EWFT proposal[11] [Fig. 8(b)]. The available data[2-4,27] are shown in Fig. 12. There is no consistent trend in the data, but one notes that the energy dependence of the $\beta(1)/\alpha$ ratio appears to follow that of the computed EW curves [Figs. 12(b) and 12(d)]. Contrary to the BL curves, the absolute magnitudes of the EW curves are quite sensitive to the f and ω values used in Eq. (15). As shown by Hagmann *et al.*,[3] there can be major deviations of these values from the tabulated ones,[25] because of excitation or stripping in the L and M shells of the projectile and target atoms. Hence we can only tentatively conclude from Fig. 12 that the $3d\sigma$ MO may correlate according to

the EWFT scheme.[11] More experimental evidence is needed to establish the correlation.

IV. $4f\sigma$-VACANCY-PRODUCTION CROSS SECTION

According to our model, the $4f\sigma$-vacancy-production cross section near symmetry is given by the summed L-vacancy-production cross section of both collision partners [Eq. (4)]. We show in Fig. 13 that the experimental cross sections[4,16,28,29] appear to obey the same kind of united-atom (UA) scaling law which was found by Behnke *et al.*[21] for the $2p\sigma$-vacancy cross section and subsequently by Meyerhof[17] for the $3d\sigma$-vacancy cross section: at a given projectile velocity the cross section is a nearly unique function of the UA $Z(=Z_p+Z_t)$, independent of Z_p. (Each different symbol in Fig. 13 represents a different value of Z_p.) In Ref. 17 it was shown that a UA ionization model proposed by Briggs[30] can produce such a scaling law, but it could not be demonstrated that ionization alone is responsible for $3d\sigma$-vacancy production. The semiclassical approximation ionization amplitudes needed to apply the Briggs model to the $4f\sigma$ case are presently not available, but are being computed.[31] In systems considerably lighter than those considered here, i.e., $Z \lesssim 20$, the $4f\sigma$-vacancy production cross section has been successfully explained solely on the basis of electron promotion.[32] Electron promotion is also invoked by Lutz *et al.*,[33] who examine the threshold behavior of $\sigma_L(l)$ in Xe+Ag collisions, but Fortner *et al.*[34] suggest that $4f\sigma$ ionization is needed to explain the threshold behavior in Kr+Kr and Kr+Xe collisions.

V. DISCUSSION

We have shown that a simple molecular model can explain the basic trends of L x-ray cross sections produced in near-symmetric heavy-ion collision with $Z \gtrsim 35$. The model is based on the proposal[16] that inner-shell vacancies are formed predominantly in highly promoted MO's ($2p\sigma$, $3d\sigma$, $4f\sigma$, $5g\sigma \cdots$) at small internuclear distances and that, on the outgoing part of the collision, the vacancies are shared between the various SA subshells. For L x-ray production near symmetry the most relevant MO is the $4f\sigma$ MO.[9,10]

The projectile velocity region examined by us, corresponds, for 41-MeV Ta, to $v_p/v_L \cong 0.1$, where v_L is the Bohr L-electron velocity. Therefore, the use of a quasimolecular model of the collision process appears to be appropriate. One then expects that the long-range coupling between the $4f\sigma$ MO and the other MO's on the outgoing part of the collision should be influenced strongly by the level separation and, to a lesser degree, by the detailed structure of the MO's. This may justify use of a vacancy-sharing model such as that of Refs. 12 and 16.

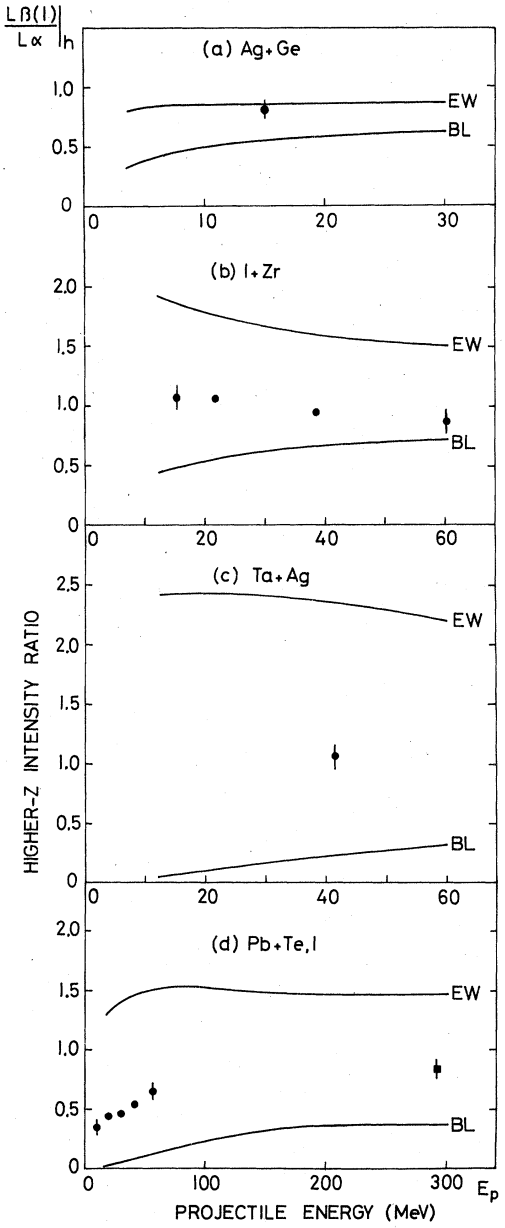

FIG. 12. $\beta(1)/\alpha$ x-ray intensity ratio for the higher-Z partner as a function of projectile energy. (a) $_{47}$Ag+$_{32}$Ge (Ref. 23), (b) $_{53}$I+$_{40}$Zr (Ref. 2), (c) $_{73}$Ta+$_{47}$Ag (Ref. 4), (d) $_{82}$Pb+$_{52}$Te, $_{53}$I (■ from Ref. 27, ● from inverse collision, Ref. 3; equivalent Pb projectile energies are shown). The curves marked BL and EW are the model results for the correlation proposals of Refs. 9 and 11, respectively.

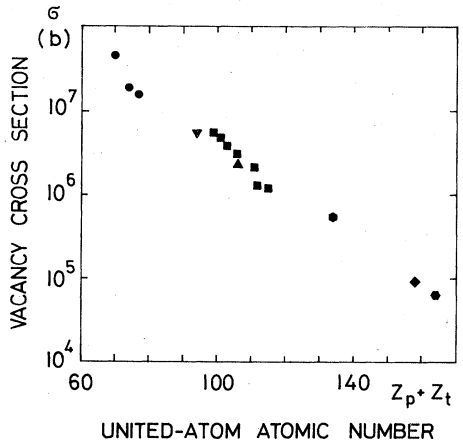

FIG. 13. Cross sections for $4f\sigma$-vacancy production at 0.49-MeV/a.m.u. projectile energy, plotted as a function of the united-atom atomic number. Experimental points: ●$_{35}$Br projectiles on various targets (Ref. 16), ▼$_{47}$Ag + Ag (Ref. 28), ■$_{53}$I projectiles on various targets (Ref. 16), ▲$_{53}$I + $_{52}$Te (Ref. 29), ⬢$_{67}$Ho + Ho, ♦$_{79}$Au + Au, ⬣$_{82}$Pb + Pb (extrapolated from Ref. 4).

Perhaps the most interesting result of the present work is the possibility of distinguishing experimentally between two correlation schemes proposed, respectively by Barat and Lichten[9] and by Eichler *et al.*[11] In terms of adiabatic level schemes, the correlations of interest in L x-ray production are determined by the nature of the avoided crossings marked 1 and 2 on Figs. 14(a) and 14(b). These figures, taken from Ref. 11, can serve as prototypes of a symmetric and an asymmetric collision system. Appropriate relativistic diagrams are presented in Refs. 35 and 36.

Our finding that at symmetry the $4f\sigma$ MO correlates to the $2p_{3/2}$ level, but that with increasing asymmetry the correlation moves to the lower-Z $2s$ level, will now be discussed from two points of view. First, we show that in region 1 in the symmetric case the crossing probability from the $3\sigma_u(4f\sigma)$ MO [in the relativistic case[35,36] called $4(\frac{1}{2})_u$] to the $2\sigma_u(3p\sigma)[3(\frac{1}{2})_u]$ MO is small, so that

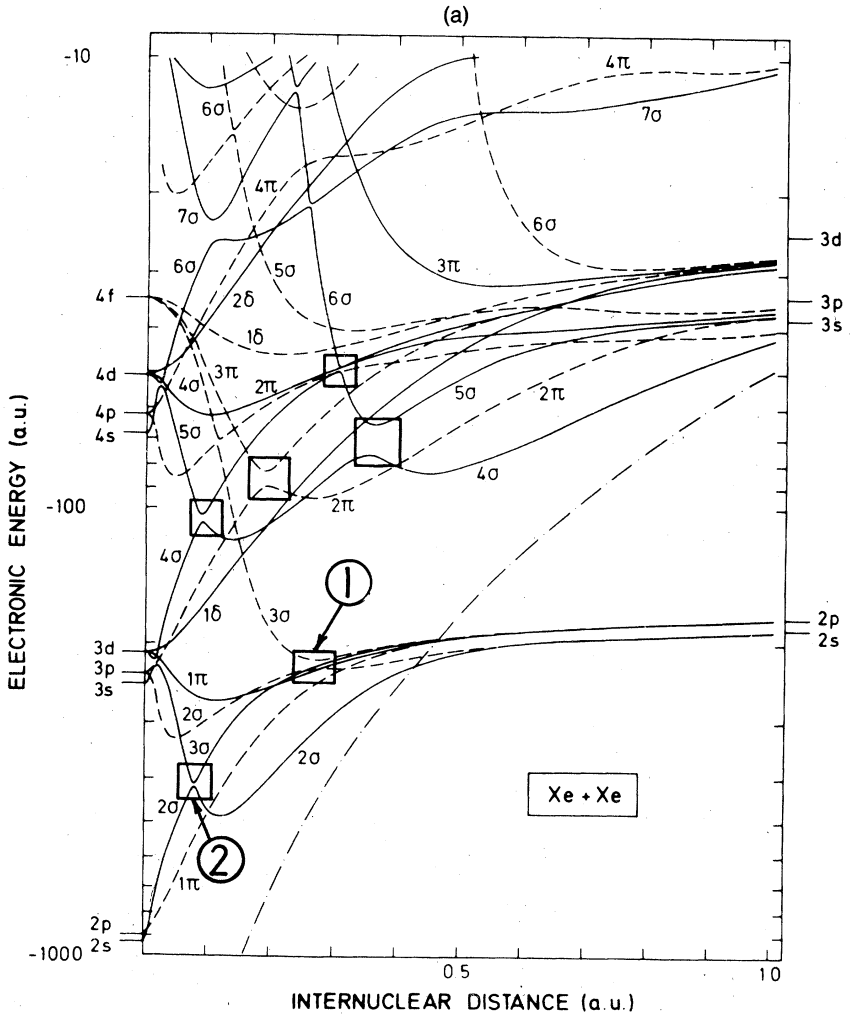

FIG. 14. Adiabatic correlation diagrams according to the nonrelativistic calculations of Eichler *et al.* (Ref. 11). (a) $_{54}$Xe + Xe. The boxed region 1 contains the $4f\sigma$-$3p\sigma$ avoided crossing ($3\sigma_u$-$2\sigma_u$, shown by dashed lines). The boxed region 2 contains the $3d\sigma$-$2s\sigma$ avoided crossing ($3\sigma_g$-$2\sigma_g$, shown by solid lines). (b) (on next page) $_{36}$Kr + $_{54}$Xe. The boxed region 1 contains the $4f\sigma$-$3p\sigma$ avoided crossing (6σ-5σ) and 2 the $3d\sigma$-$2s\sigma$ avoided crossing (4σ-3σ).

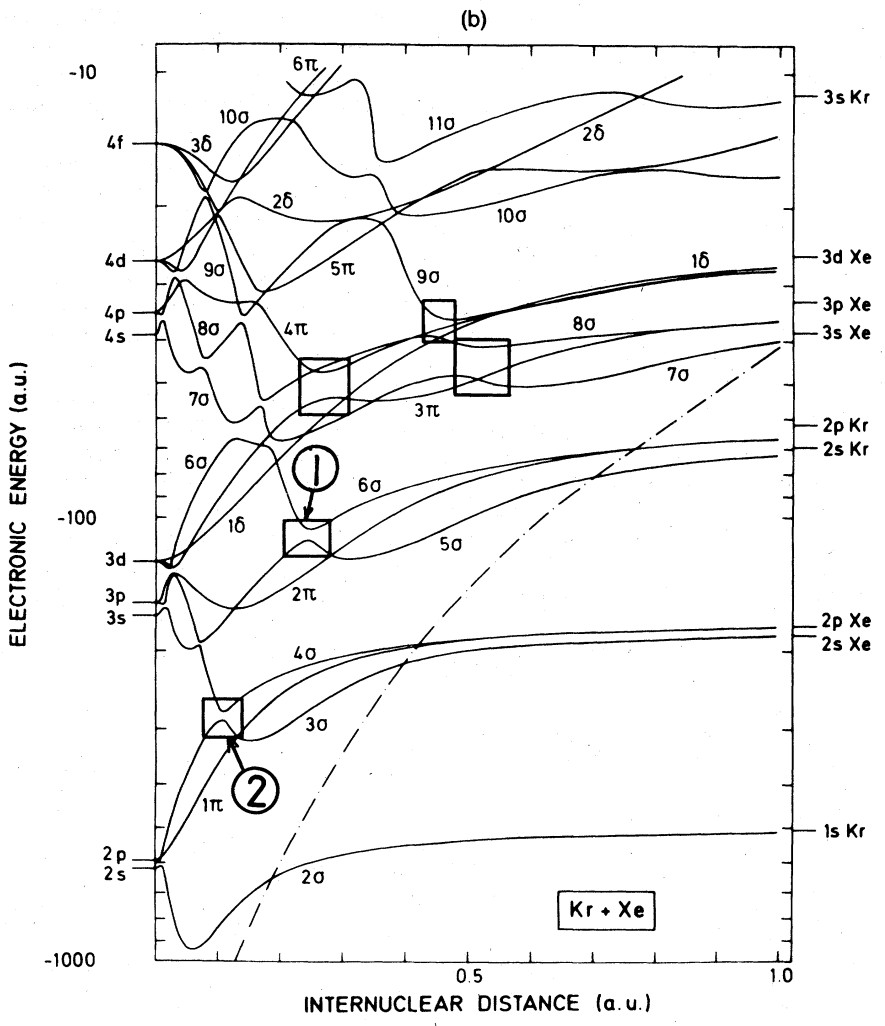

Fig. 14. *(Continued)*

the $4f\sigma$ MO is expected to follow the adabatic correlation to the SA $2p_{3/2}$ level.[9] But for a sufficiently asymmetric system the crossing probability from the $6\sigma(4f\sigma)$ to the $5\sigma(3p\sigma)$ MO increases so that the $4f\sigma$ MO tends to correlate to the lower-Z $2s$ level. [In the relativistic case,[35,36] two crossings are involved here: $8(\frac{1}{2}) \rightarrow 7(\frac{1}{2})$ and $7(\frac{1}{2}) \rightarrow 6(\frac{1}{2})$, but the latter energy gap is so narrow that only the former needs to be considered. Hagmann *et al.*[3] have considered the crossings in the relativistic case in greater detail.] Second, we show that the nature of the avoided $4f\sigma$-$3p\sigma$ crossing 1 changes drastically with symmetry as the result of a rapidly changing Stark effect.[9,11] The situation for the avoided $3d\sigma$-$2s\sigma$ crossing 2, which determines the $3d\sigma$ correlation, seems to be quite different.

A quantitative estimate of the crossing probability between two adiabatic MO's can be obtained from the Landau-Zener formula.[37] Following Eichler *et al.*,[11] we write the Landau-Zener crossing probability at a projectle velocity v_p as

$$P = (\tfrac{1}{2})^{v_c/v_p}, \tag{38}$$

where

$$v_c = \frac{2\pi}{\ln 2} \frac{|H_{12}|^2}{\Delta(\partial\epsilon/\partial R)}. \tag{39}$$

Here H_{12} is equal to one-half of the minimum-energy splitting between the adiabatic energy curves $E_1(R)$ and $E_2(R)$ and $\Delta(\partial\epsilon/\partial R)$ is the difference in slopes between the diabatic curves $\epsilon_1(R)$ and $\epsilon_2(R)$ at the crossing point. If v_c is larger than v_p one expects a small transition probability, i.e., a correlation according to the BL proposal[9] in the case considered here. If v_c is considerably smaller than v_p, one expects a large transition probability, i.e., a correlation according to the EWFT proposal.

Using information kindly furnished to us by the

TABLE I. Landau-Zener critical velocity and subshell to Stark splitting ratio.

Avoided crossing [a]	System	$\frac{Z_l}{Z_h}$	v_c(VSM) (a.u.)	Reference [b]	v_c(HFD) [c] (a.u.)	$\frac{\Delta W}{\Delta E}$
$4f\sigma$-$3p\sigma$ (region 1)	Xe-Xe	1	0.15, 1.3	11, 35	···	0.50
	Kr-Kr	1	0.8	11	···	0.45
	Ag-Xe	0.87	···	···	0.9	0.29
	I-Au	0.67	0.2	35	4.1	0.14
	Kr-Xe	0.67	0.1	11	···	0.13
$3d\sigma$-$2s\sigma$ (region 2)	Xe-Xe	1	0.01, 0.06	11, 35	···	0.09
	Kr-Kr	1	0.02	11	···	0.08
	Ag-Xe	0.87	···	···	1.1	0.12
	I-Au	0.67	1.5	35	2.0	0.31
	Kr-Xe	0.67	0.04	11	···	0.20

[a] See Figs. 14 and 15.
[b] Energy curves of Ref. 11 have been computed nonrelativistically; others, relativistically.
[c] Reference 36.

authors of Refs. 11, 35, and 36, we have obtained v_c for the crossing region 1 in Fig. 14. Table I gives the results. Unfortunately, the variable screening model (VSM) used in Refs. 11 and 35 are the Hartree-Fock-Dirac model (HFD) used in Ref. 36 give widely divergent results, so that a quantitative application of Eq. (38) is not meaningful. Nevertheless, one sees that the VSM is in qualitative accord with our findings, in that v_c tends to decrease with increasing asymmetry: this signals a shift toward the EWFT correlation scheme. Our projectile velocities correspond to $v_p \cong 2-3$ a.u. Hence our findings for the shift in the $4f\sigma$ correlation (Sec. III) would require $v_c \gtrsim 3$ a.u. for symmetric collisions and $v_c \lesssim 2$ a.u. for sufficiently asymmetric collisions. We note that Nikulin and Guschina[38] find no evidence for any $4f\sigma$-$3p\sigma$ avoided crossing in the Kr+Kr system. In the language of Eq. (38) this would correspond to a very large value for v_c.

According to the VSM,[11] the $3d\sigma$-$2s\sigma$ crossings in region 2 are all characterized by very small values of v_c, listed in Table I. The HFD model[36] gives much larger values. A similar effect was found in a comparison of the VSM and HF results for the same crossing in Ne+Ne.[39] Nevertheless the generally smaller values of v_c in region 2 as compared to region 1, suggest a tendency toward the EWFT scheme. Unfortunately the experimental evidence (Fig. 12) is not conclusive.

Returning to $4f\sigma$-$3p\sigma$ avoided crossing regions 1 in Figs. 14(a) and 14(b) one may now inquire which physical features of the collision system determine the trend of the $4f\sigma$ correlation, as the asymmetry of the system changes. Following suggestions of Barat and Lichten,[9] Eichler *et al.*[11] have explored the competing roles of the Coulombic one-electron Stark splitting ΔE and of the $2p$-$2s$ subshell splitting ΔW, in determining whether a given correlation follows the BL or EWFT schemes. Figure 15, adapted from Ref. 11, illustrates the argument: as ΔE increases from small values (with respect to ΔW) to large values, the avoided crossing should become increasingly dia-

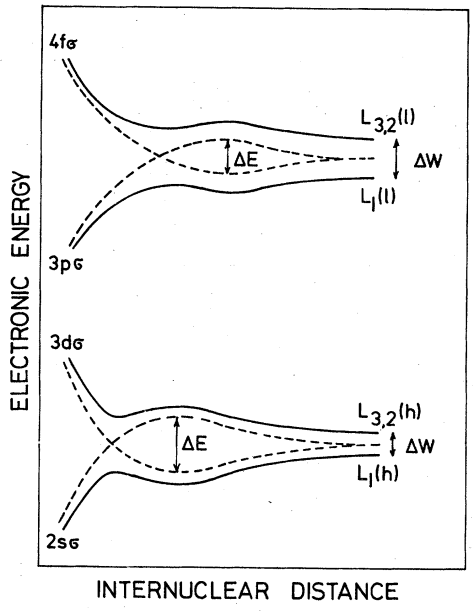

FIG. 15. Schematic diagram for the adiabatic correlations to the L levels of the lower-Z (l) and higher-Z (h) collision partners in a slightly asymmetric system (adapted from Ref. 11). The Coulombic Stark splitting is denoted by ΔE and the $2p$-$2s$ subshell splitting by ΔW. Dashed curves show the energy levels for a one-electron system. Solid curves illustrate the situation for a screened system.

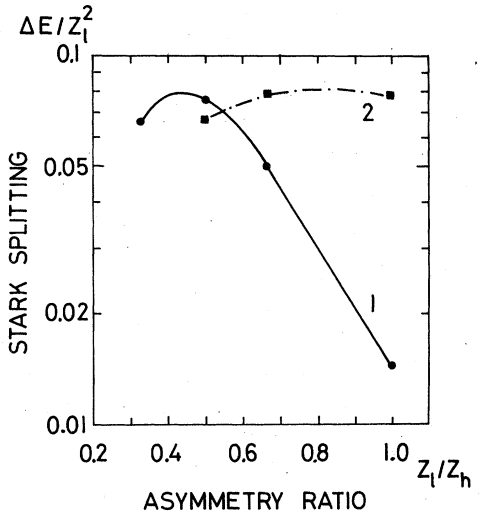

FIG. 16. Coulombic Stark splitting ΔE for a one-electron, two-center system as a function of the asymmetry ratio Z_l/Z_h. Points are computed from Ref. 40. Curve 1 applies to the $4f\sigma$-$3p\sigma$ splitting, curve 2 to the $3d\sigma$-$2s\sigma$ splitting (see Fig. 15).

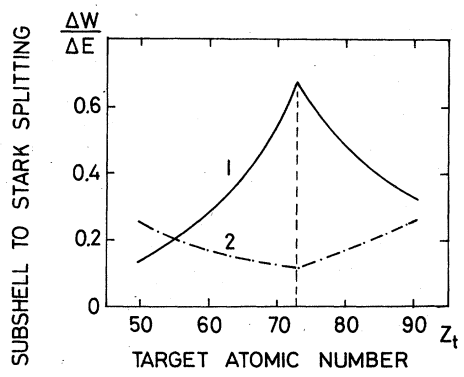

FIG. 17. Subshell to Stark splitting ratio for $_{73}$Ta projectiles bombarding various targets, plotted as a function of the target atomic number. Vertical dashed line indicates symmetry. Curve 1 applies to the $4f\sigma$-$3p\sigma$ MO's, curve 2 to the $3d\sigma$-$2p\sigma$ MO's (see Fig. 15). According to Ref. 11, as $\Delta W/\Delta E$ decreases, the MO correlations are expected to change from adiabatic to diabatic.

batic, i.e., the correlation should shift increasingly from the BL to the EWFT scheme.

To put this criterion on a quantitative basis we have calculated the ratio $\Delta W/\Delta E$ as a function of the asymmetry of the system, for the MO's correlating to the lower-Z and higher-Z L levels. To obtain the Coulombic one-electron $4f\sigma$-$3p\sigma$ and $3d\sigma$-$2s\sigma$ Stark splittings ΔE, we have used the calculations of Hartmann and Helfrich.[40] Figure 16 gives their values of $\Delta E/Z_l^2$ as a function of Z_l/Z_h, which allow approximate interpolation for any collision pair Z_l, Z_h. The $2p$-$2s$ subshell splittings ΔW were computed from tabulations.[41] Figure 17 shows the resultant values of $\Delta W/\Delta E$ for Ta projectiles. For other projectiles similar results are obtained. One sees that for the $4f\sigma$-$3p\sigma$ case (curve 1), the value of $\Delta W/\Delta E$ peaks at symmetry and drops rapidly with increasing asymmetry. This is in qualitative accord with our findings: at symmetry, the large value of $\Delta W/\Delta E$ leads to the expectation of BL correlation ($4f\sigma \rightarrow L_3$); the decreasing values of $\Delta W/\Delta E$ with increasing asymmetry lead to the expectation of increasing EWFT correlation $[4f\sigma \rightarrow L_1(l)]$. The trend appears to be in accord with the overall trend of v_c for region 1 given in Table I, where we list also the values of $\Delta W/\Delta E$ for each collision pair.

For the $3d\sigma$-$2s\sigma$ case, curve 2 in Fig. 17, the ratio $\Delta W/\Delta E$ is small throughout the region near symmetry. This leads to the expectation of EWFT correlation $[3d\sigma \rightarrow L_1(h)]$ in the entire region. As discussed above, experimentally this is not definitely ascertained (Fig. 12).

By comparing the numerical values of $\Delta W/\Delta E$ and v_c one can, for a given model, establish an approximate one-to-one relationship (Table I). This simply indicates quantitatively that a weak Stark splitting leads to a broad avoided crossing with a large gap (BL correlation), whereas a strong Stark splitting leads to an avoided crossing with a small gap (EWFT correlation). From Fig. 16 one can see that our findings for the $4f\sigma$ correlation find a natural explanation in terms of the rapid increase of the Stark splitting as the asymmetry of the system increases. The experimental features of the $3d\sigma$ correlation must be investigated further. From a theoretical point of view there is a need to establish the validity of various MO calculations and then to compute the actual couplings between the $4f\sigma$ MO and the MO's leading to the lower-Z subshells. Similarly the couplings between the $3d\sigma$ MO and the higher-Z subshells must be calculated, as has been done in Refs. 42 and 43 for the Ne-Ne system.

ACKNOWLEDGMENTS

We are most grateful to G. Presser, S. Hagmann, A. Schoenfeldt, and P. H. Mokler who sent us data prior to publication and to B. Fricke and U. Wille who provided us with numerical information for the calculation of the Landau-Zener critical velocity. Discussions with R. Anholt and R. J. Fortner were most helpful. One of us (W.E.M)

gratefully acknowledges receipt of a Tenured Faculty Development Award, supported by Lilly Endowment, Inc., from Stanford University, and the hospitality of the Laboratory for Nuclear Physics of the Swiss Federal Institute of Technology during a four-month stay there. This work was partly supported by the U. S. NSF and by the Swiss National Science Foundation.

---

*Present address: Institut de Physique de l'Université de Fribourg, Pérolles, 1700 Fribourg, Switzerland.

[1]T. L. Hardt and R. L. Watson, At. Data Nucl. Data Tables 17, 107 (1976).

[2]S. Datz, C. D. Moak, B. R. Appleton, M. D. Brown, and T. A. Carlson, in *Electronic and Atomic Collisions*, edited by L. M. Branscomb *et al.* (North-Holland, Amsterdam, 1971), p. 409 [in this work, cross section measurements between Zr and La were affected by target-mounting difficulties: S. Datz, (private communcation)]; S. Datz, C. D. Moak, B. R. Appleton, and T. A. Carlson, Phys. Rev. Lett. 27, 363 (1971). Similar measurements are reported by P. Mokler and H. J. Stein [Annual Report of the Nuclear Physics Facility, Jülich, Germany (1971), p. 197 (unpublished)].

[3]S. Hagmann, P. Armbruster, G. Kraft, P. H. Mokler, and H. J. Stein, Z. Phys. A 288, 353 (1978); 290, 25 (1979).

[4]A. Rüetschi, Ph.D. thesis (Swiss Federal Institute of Technology, Zurich, 1977) (unpublished).

[5]P. Armbruster, Z. Phys. 166, 341 (1962).

[6]P. Armbruster, E. Roeckl, H. J. Specht, and A. Vollmer, Z. Naturforsch. 19a, 1301 (1964).

[7]H. J. Specht, Z. Phys. 185, 301 (1965).

[8]T. M. Kavanagh, M. E. Cunningham, R. C. Der, J. Fortner, J. M. Khan, J. Zaharis, and J. D. Garcia, Phys. Rev. Lett. 25, 1473 (1970).

[9]M. Barat and W. Lichten, Phys. Rev. A 6, 211 (1972).

[10]R. J. Fortner, Phys. Rev. A 10, 2218 (1974); see also H. Oona, J. D. Garcia, and R. J. Fortner, *ibid.* 16, 525 (1977).

[11]J. Eichler, U. Wille, B. Fastrup, and K. Taulbjerg, Phys. Rev. A 14, 707 (1976).

[12]W. E. Meyerhof, Phys. Rev. Lett. 31, 1341 (1973).

[13]J. S. Briggs and K. Taulbjerg, J. Phys. B 8, 1909 (1975); and 9, 1641 (1976).

[14]K. Taulbjerg, J. Vaaben, and B. Fastrup, Phys. Rev. A 12, 2325 (1975).

[15]W. N. Lennard and I. V. Mitchell, J. Phys. B 9, L 317 (1976); W. N. Lennard, I. V. Mitchell, J. S. Forster, and D. Phillips, *ibid.* 10, 2199 (1977).

[16]W. E. Meyerhof, R. Anholt, J. Eichler, and A. Salop, Phys. Rev. A 17, 108 (1978).

[17]W. E. Meyerhof, Phys. Rev. A 18, 414 (1978).

[18]Yu. N. Demkov, Zh. Eksp. Theor. Fiz. 45, 195 (1963) [Sov. Phys.-JETP 18, 138 (1964)].

[19]E. E. Nikitin, Opt. Spektrosk. (USSR) 13, 761 (1962) [Opt. Spectrosc. (USSR) 13, 431 (1962)]; and Adv. Quantum Chem. 5, 135 (1970).

[20]P. H. Woerlee, R. J. Fortner, S. Doorn, Th. P. Hoogkamer, and F. W. Saris, J. Phys. B 11, L 425 (1978).

[21]H. H. Behnke, P. Armbruster, F. Folkmann, S. Hagmann, J. R. Macdonald, and P. H. Mokler, Z. Phys. A 289, 333 (1979).

[22]W. E. Meyerhof, R. Anholt, and T. K. Saylor, Phys. Rev. A 16, 169 (1977).

[23]G. Presser (private communication).

[24]By very careful decomposition of the L_γ line group it is possible to extract separate L_1 and L_2 vacancy cross sections. See J. Tanis, B. Budick, J. W. Kast, and A. M. Rushton, Phys. Rev. A (to be published). Also, in some cases the L_η line can be used to obtain the L_2-vacancy cross section [A. Schoenfeldt and P. H. Mokler (private communication)].

[25]W. Bambynek, B. Crasemann, R. W. Fink, H. U. Freund, H. Mark, C. D. Swift, R. E. Price, and P. V. Rao, Rev. Mod. Phys. 44, 716 (1972).

[26]J. H. Scofield, At. Data Nucl. Data Tables 14, 121 (1974).

[27]A. Schoenfeldt and P. H. Mokler (private communication).

[28]M. Stöckli, Ph.D. thesis (Swiss Federal Institute of Technology, Zurich, Switzerland, 1978) (unpublished).

[29]H. J. Stein, H. O. Lutz, P. H. Mokler, and P. Armbruster, Phys. Rev. A 5, 2126 (1972).

[30]J. S. Briggs, J. Phys. B 8, L 485 (1975); and Rep. Prog. Phys. 39, 217 (1976).

[31]L. Kocbach (private communication).

[32]G. B. Schmid and J. D. Garcia, Phys. Rev. A 15, 85 (1977).

[33]H. O. Lutz, W. R. Murray, R. Pretorius, T. Morović, B. Fricke, W. D. Sepp, and I. J. van Heerden, J. Phys. B 11, 2527 (1978).

[34]R. J. Fortner, P. Woerlee, and F. W. Saris, J. Phys. B 11, L697 (1978).

[35]P. Kaufmann and U. Wille, Z. Phys. A 279, 259 (1976).

[36]B. Fricke, T. Morović, W. D. Sepp, A. Rosén, and D. E. Ellis, Phys. Lett. 59A, 375 (1976); T. Morović, B. Fricke, W. D. Sepp, A. Rosén, and D. E. Ellis, *ibid.* 63A, 12 (1977).

[37]M. R. C. McDowell and J. P. Coleman, *Introduction to the Theory of Ion-Atom Collisions* (North-Holland, Amsterdam, 1970), p. 181ff.

[38]V. K. Nikulin and N. A. Guschina, J. Phys. B 11, 3553 (1978).

[39]T. Anderson, E. Bøving, P. Hedegaard, and J. Østgaard Olsen, J. Phys. B 11, 1449 (1978).

[40]H. Hartmann and K. Helfrich, Theor. Chim. Acta (Berlin) 10, 406 (1968); K. Helfrich and H. Hartmann, *ibid.* 16, 263 (1970).

[41]J. A. Bearden and A. F. Burr, *Atomic Energy Levels*, Report No. NYO-2543-1, U.S. D.O.E., Division of Technical Information (National Technical Information Service, U. S. Department of Commerce, Springfield, Va., 1965).

[42]R. Albat, N. Gruen, and B. Wirsam, J. Phys. B 8, 2520 (1975).

[43]W. Fritsch and U. Wille, J. Phys. B 11, 4019 (1978).